The Existence and Vertical Structure of Fast, Eastward-Moving Disturbances in the Equatorial Troposphere

RALPH F. MILLIFF AND ROLAND A. MADDEN

National Center for Atmospheric Research, Boulder, Colorado*

(Manuscript received 30 March 1995, in final form 17 August 1995)

ABSTRACT

Eastward phase propagation, at speeds faster than 30 m s^{-1}, of a signal in the equatorial troposphere of the Eastern Pacific is detected, first in historical meteorological observations and then in more recent data. A first baroclinic mode vertical structure is identified with this signal in separate analyses based on linear theory and complex empirical orthogonal functions, respectively. This rapid, eastward signal is conceptualized as a far-field dispersion product of strong convection associated with the intraseasonal tropical oscillation in the Indian Ocean and Western Pacific.

1. Introduction

The schematic produced by Madden and Julian (1972a, their Fig. 16) to demonstrate important features of the intraseasonal tropical oscillation (ITO; called 40–50 day tropical oscillation in their paper) indicates a slow-moving buildup of convection over the equatorial Indian Ocean, then eastward movement of the convection at about 6 m s^{-1} to the Central Pacific where it weakens and dies. In addition, there is evidence in the schematic[1] of an accompanying pressure anomaly that is manifest both in the zonal average and in a fast, eastward-moving component of about 20 m s^{-1}.

In this paper we examine more carefully this fast, eastward propagating signal associated with the ITO. To direct our analysis we invoke a simple conceptual model of the fast surface-pressure signal as the manifestation of a dispersion product from the initiation or enhancement of an ITO somewhere in the equatorial Indian Ocean. Consider a large-amplitude convection event as a single-point perturbation of some idealized equilibrium condition along the equatorial waveguide. According to classical adjustment theory, the broadband initial response close to the perturbation will disperse such that remote locations receive, sequentially, wave-packet components of the initial response. We identify these packets here as dispersion products and note for the purposes of later discussion that the individual dispersion products that emanate from a given perturbation need not themselves be dispersive.

We imagine that the dispersion product that projects onto the surface pressure wave has originated in the active convective region of the Indian Ocean or Western Pacific and propagated far enough to be identified as an unique signal in the Central and Eastern Pacific region, where the convection is weakened or completely decayed. In this way, we will refer to the equatorial Indian Ocean and Western Pacific as the forcing region and to the equatorial Eastern Pacific as the propagating region. A similar two-regime character has been considered in a number of previous studies (e.g., Knutson et al. 1986; Lau and Peng 1987; Hayashi and Miyahara 1987; Hendon 1988; Gutzler and Madden 1989). Given the rapid eastward propagation of the surface-pressure anomaly in the propagating region, we anticipate a relatively large scale-depth and relatively few (if any) zero crossings in the vertical structure of this signal in the troposphere.

In the next section we examine the surface pressure signal as it occurs in cross spectra from historical and more recent meteorological station observations in the propagating region of the Pacific. We estimate a vertical structure for this signal from linear theory. This estimate is compared with an independent estimate from a complex empirical orthogonal function (cEOF) analysis of observed data. The implications of oversimplifications in our conceptual model are discussed in

* The National Center for Atmospheric Research is sponsored by the National Science Foundation.

[1] The schematic in Madden and Julian (1972a) is probably not adequate to define precisely this eastward phase velocity. However, it is sufficient to demonstrate that eastward propagation of the surface pressure anomaly is faster than the eastward propagation of the cloud system tied to the convection.

Corresponding author address: Dr. Ralph F. Milliff, National Center for Atmospheric Research, P.O. Box 3000, Boulder, CO 80307-3000.

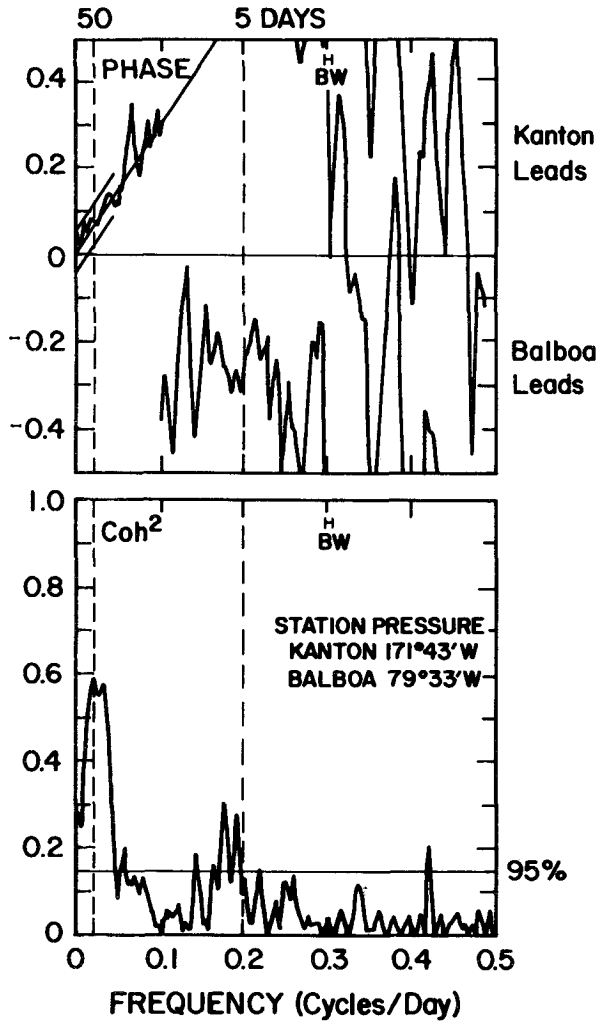

FIG. 1. Coherence squared (bottom) and phase in fractions of a cycle between the surface pressures at Kanton Island (2.8°S, 171.7°W) and Balboa, Panama, (9.0°N, 79.6°W) for the period 16 December 1959–24 March 1967 (2656 days). The bandwidth and the 95% limit for a null hypothesis of zero coherence are indicated (the 95% limit in Madden and Julian 1994 was mistakenly placed at a level for twice the actual number of available degrees of freedom). The straight line in the phase diagram indicates phases associated with a constant 3-day delay between Kanton and Balboa. The 95% confidence limits for phase are based on average squared coherence of 0.5 between 0 and 0.05 cpd and 42 degrees of freedom (Jenkins and Watts 1968, 381). [Adapted from Madden and Julian (1994), their Fig. 1.]

the third section, and conclusions are drawn in the final section of this paper.

2. Analyses

a. *Surface pressure cross spectra and lag-correlations*

Madden and Julian (1994) noticed more rapid eastward propagation of surface pressure relative to other features of the ITO. Coincident time series of daily surface-pressure observations were obtained from the rawinsonde records at Kanton Island[2] (2.8°S, 171.7°W) and Balboa, Panama, (9.0°N, 79.6°W) for a 7-yr period (2656 days) beginning in 1959. Values were taken from the first available sounding for each day. For days when there were no observations, an estimate was made from a linear interpolation in time. Cross-spectra were computed by first Fourier transforming each series. Next, the resulting coefficients were squared or multiplied together and these squares and products were then smoothed with a running average of 21 discrete frequencies, after adjusting raw estimates to remove the seasonal variation.[3] This results in spectral values with a frequency resolution of 0.008 cycles per day (cpd) and 42 degrees of freedom, based on the optimistic assumption that each datum is independent. Estimates of the squared coherence and phase relation determined from these time series are depicted in Fig. 1 (adapted from Madden and Julian 1994; their Fig. 1). The coherence is strongest in the low-frequency range corresponding to a period of around 50 days. Coherence exceeds the 95% confidence criterion over a broad, low-frequency band up to about 0.05 cpd. The coherence is also strong for periods slightly longer than 5 days.

The phase as a function of frequency demonstrates that over the statistically significant lower-frequency band, the surface pressure at Kanton Island leads that at Balboa, supportive of eastward propagation. In the band around 5-day period, the pressure at Balboa leads, suggesting westward propagation. This feature has been identified as the 5-day global-scale Rossby wave (e.g., Madden and Julian 1972b). The accuracy in the estimate of the phase angle at a given frequency is a function of the magnitude of the squared coherence at that frequency. We see in Fig. 1 that for the strongest coherence around 50-day period, the phase is a linear function of frequency. As the coherence drops in the vicinity of 20-day period, the phase becomes noisier but remains a roughly linear function of frequency out to 10-day period. This linear relationship is indicative of an eastward propagating signal in surface pressure with a constant delay between the stations. From the slope of the linear relation, we estimate the delay to be near three days suggesting a phase speed of about 39 $m\ s^{-1}$, within a factor of 2 of that suggested by the schematic of Madden and Julian (1972a).

If our simple conceptual model of a dispersion product is appropriate, then Fig. 1 implies that the discrete local frequencies resulting from the wave packet are

[2] Formerly Canton Island.

[3] Raw spectral estimates at the two harmonics nearest the annual and semiannual frequencies were removed and replaced by a linear interpolation between adjacent estimates.

each associated with discrete wavenumbers within the packet so that a single phase velocity for the dispersion product is achieved. This model is purposefully different from a model that invokes a single propagating pure mode because the phase angles of Fig. 1 indicate that a band of frequencies (0 to 0.1 cpd) are involved, and they demonstrate a constant delay between Kanton and Balboa. In our conceptual model, the frequency and wavenumber pairs within the packet do not change as a function of time; that is, the dispersion product is itself nondispersive.

We can look for the constant delay in a simpler statistic: the lag-correlation between the pressure records at the two stations. Figure 2 shows that the lag-correlation maximizes at 4 days (all data) and at 3 days for the low-pass filtered data meant to capture the low-frequency range of high coherence (Fig. 1). The response of the low-pass filter is indicated in Fig. 2. The station data used in the lag-correlation calculation were extended back to 1 December 1956 and forward to 27 January 1967, providing time series of 3700 days. At Kanton and Balboa fewer than 1% of days had no observations, and these days were not included in this calculation.

Note that the lag-correlations at zero lag are nonzero for the unfiltered and low-pass filtered series. This implies a very large-scale surface pressure variation that we can think of as being zonally symmetric, at least over the limited range of the Eastern Pacific region spanned by Kanton Island and Balboa. If we assume that every tenth datum represents an independent observation, then a conservative estimate of the 95% confidence interval about zero correlation in Fig. 2 is on the order of ±0.10 (Panofsky and Brier 1963). This confidence interval narrows and becomes asymmetric as the true correlation increases from zero. Therefore, although the 2–4-day correlations are significantly different from zero (Fig. 2), it is not certain that they are significantly different from the zonally symmetric signal (at 0 lag). Nonetheless, the maximum correlation at 3-day lag is consistent with the statistically significant inferences drawn from the cross spectrum in Fig. 1.

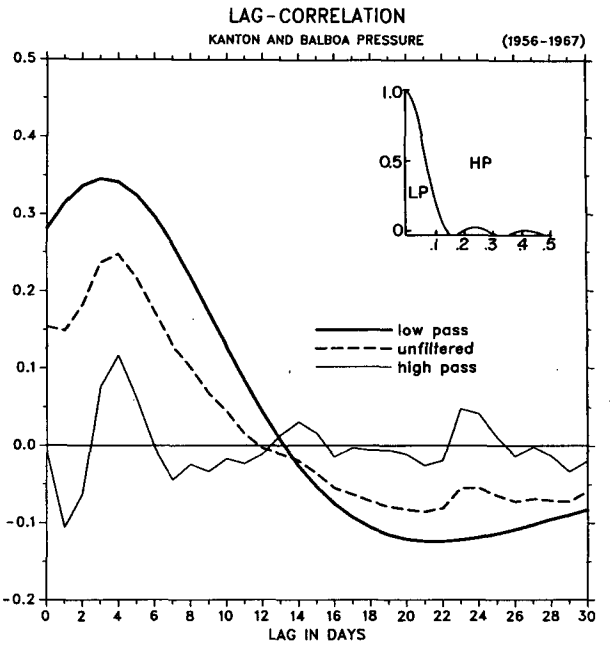

FIG. 2. Lag-correlations in days for surface pressures between Kanton Island and Balboa for the period 1 December 1956–24 March 1967 (3700 days). The dashed curve marks lag-correlations for unfiltered data, the thick curve for low-pass filtered data, and the thin curve for high-pass filtered data. The low-pass filter response is indicated in the insert. The high-pass filter response is one minus the low-pass response. A conservative estimate of the 95% significance interval about zero correlation is 0.10.

b. *Recent data*

We can also look for confirmatory evidence of the rapidly propagating signal in more recent data. Rawinsonde observations at Kanton were discontinued in 1967 and restarted in 1990, but there are too many missing observations in this recent record to permit analyses exactly parallel to those of Figs. 1 and 2. Instead, we have examined a 7-yr record of station pressure at Howard AFB (8.9°N, 79.6°W) near Balboa and sea level pressure at Kanton that is contained in the surface synoptic dataset. Sea level and station pressure are nearly identical at Kanton since the station elevation is only 2 m. These data originated from the National Meteorological Center decode of the Global Telecommunications System Transmissions. They are available in the NCAR archives at 0000, 0600, 1200, and 1800 UTC. We averaged all available data for each day to build 2556-day time series over the period 1985–1991. At Howard AFB there were no days without some data, while 6% of the days at Kanton Island had no data. Again, for cross spectra missing data were approximated by linear interpolations in time, and these dates were not included in the lag-correlation computations.

Figure 3 shows estimates of the squared coherence and phase as in Fig. 1 for the 1985–1991 data. The coherence is again large at the lowest frequencies, and statistical significance for rejecting a zero-coherence null hypothesis extends to at least 0.05 cpd. The linear increase in phase angle with frequency is not as evident as it is in Fig. 1; however, one can still make a case that it exists out to 20-day period.

Figure 4 is the lag-correlations for the 1985–1991 data. Note the change in ordinate between Figs. 2 and 4. The higher correlations evident in the 1985–1991 data are not investigated further in this paper; however, we note that the recent surface synoptic observations are of higher quality in that there are often four obser-

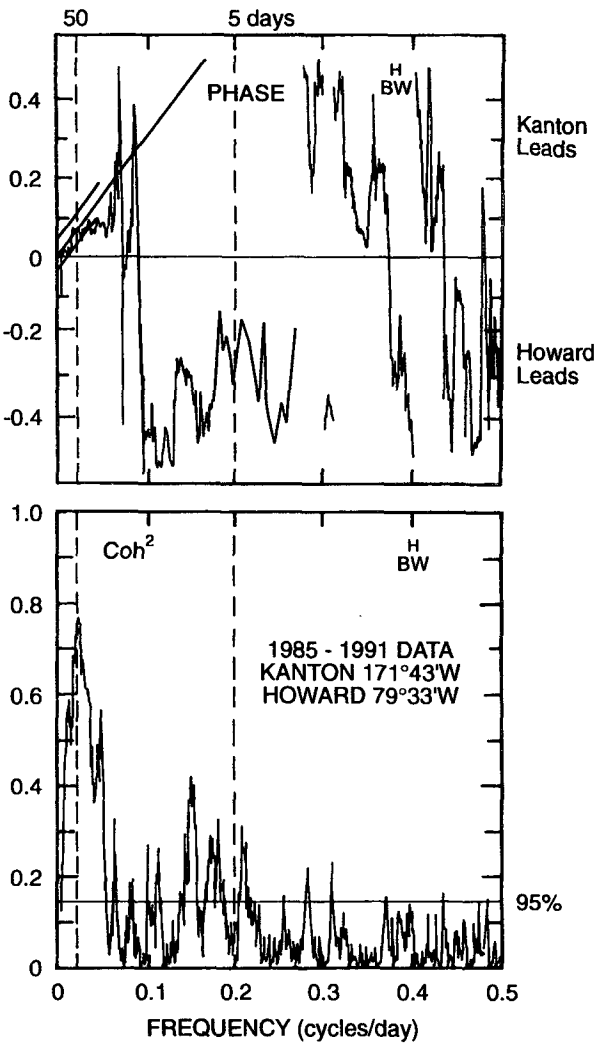

FIG. 3. Coherence squared (bottom) and phase in fractions of a cycle between sea level pressures at Kanton Island and station pressure at Howard AFB (8.9°N, 79.6°W) near Balboa for a period of 2556 days over the interval 1985–1991. Confidence limits and bandwidth as in Fig. 1.

vations available to form a daily average, while only pressure from the first available rawinsonde was used for each day in the older dataset.[4] Also, a visual inspection of the older data indicated that the recorded pressures were often rounded to the nearest whole hectopascal. In the case of the early part of the Balboa record, it appeared that pressures were not recorded below 1000 hPa. Again, the lag correlation maximizes at four days (unfiltered) and at two and three days for the low-pass filtered data. When we computed the lag-correlations based on the six-hourly data, that is, without making daily averages, the maximum value was at 3.5-day lag. This suggests phase speeds of 34 m s^{-1}.

c. *Vertical structure equation*

These rapid phase speed estimates can be compared with a simple theoretical estimate from the decomposition of wind and geopotential height profiles into vertical modes via the vertical structure equation. This approach is well known. In our application we adopt the conventions and notation of Silva-Dias (1986). We require the usual linear assumption on the dynamics, and we consider the presence of a lid at the top of the atmospheric column (i.e., at 100 hPa).

Assume that station wind and geopotential height can be separated into vertical and horizontal parts as

$$\begin{bmatrix} u' \\ v' \\ z' \end{bmatrix}(\lambda, \phi, \sigma, t) = \xi(\sigma) \cdot \begin{bmatrix} \hat{u} \\ \hat{v} \\ \hat{z} \end{bmatrix}(\lambda, \phi, t),$$

where the independent variables are longitude λ, latitude ϕ, (nondimensional) pressure surface σ, and time

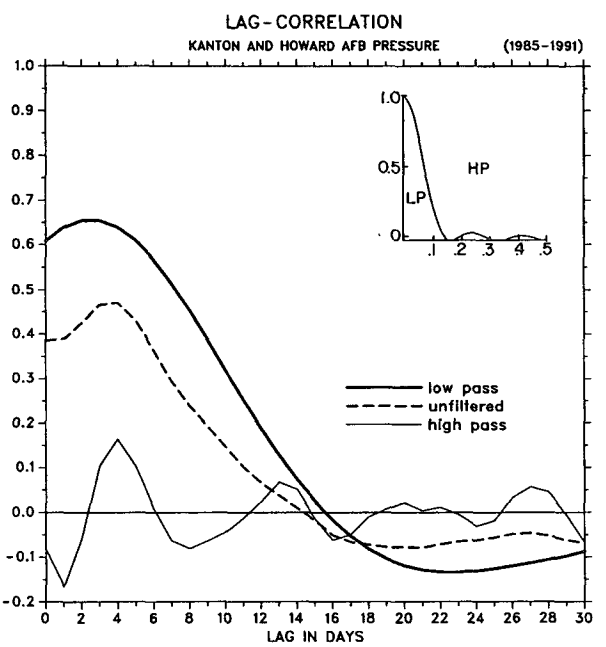

FIG. 4. Lag-correlations in days between sea level pressures at Kanton Island and station pressure at Howard AFB for the period 1985–1991 (2556 days). The filter characteristics are identical to those depicted in Fig. 2 (insert). Note the change in scale on the ordinate with respect to Fig. 2.

[4] As a test, we took only the first available observation for each day of the 1985–1991 data and computed lag-correlations. Results for the unfiltered data were similar in character to those of Fig. 4, but reduced in magnitude by about 0.1. It should be noted that this test is not perfect since the first available observation in the recent data was nearly always 0000 UTC, while that from rawinsonde data was often 1200 UTC or, less often, some other rawinsonde release time.

t. The dependent variables are the wind vector components u', v', and the geopotential height z'. Their horizontal projections are $\hat{u}, \hat{v}$, and $\hat{z}$, respectively. The horizontal modes are solutions to the Laplace tidal equations that can be separated into three classes of wave types (e.g., Longuet-Higgins 1968; Kasahara and Puri 1981): westward propagating Rossby waves; westward-propagating inertia–gravity waves; and eastward-propagating inertia–gravity waves. In our problem, Kanton leads Balboa (Fig. 1), so we will focus on the eastward propagating class. A special case for an inertia–gravity wave at the equator is the equatorial Kelvin wave, which fits well with the nondispersive character indicated by Fig. 1.

Within the context of this modal decomposition we are modifying the dispersion-product conceptual model described previously. The modal decomposition yields sets of orthogonal structures in the vertical and horizontal within which we hope a very few structures account for large fractions of the variability in the station data, thereby inferring dominant spatial and temporal scales. In practice, the sets of orthogonal structures are finite. The number of vertical modes depends on the number of levels in the vertical discretization, and the number of horizontal modes that can be represented for each eigenvalue depends on the resolution in the horizontal (e.g., the spectral truncation). We do not expect to resolve each wavenumber or frequency implied by the dispersion-product notion raised earlier of a nondispersive, broadband wave packet. Rather, the modal decomposition might resolve the large-scale envelope that bounds the wave packet. Constrained by the vertical resolution and the assumptions inherent in the theory, this envelope is treated as a single, dominant Kelvin-mode for our problem. Again, the Kelvin wave itself is nondispersive. We assume that it comprises the dispersion product of interest (of many possible dispersion products) in response to strong convection associated with the ITO.

The projections in the vertical are given by $\xi(\sigma)$, which is governed by the following ordinary differential equation of Sturm–Liouville form:

$$\frac{d}{d\sigma}\left[F\left(\bar{T}, \frac{d\bar{T}}{d\sigma}\right)\frac{d\xi}{d\sigma}\right] + \frac{1}{D}\xi = 0, \qquad (1)$$

with boundary conditions

$$\frac{d\xi}{d\sigma} = 0; \quad \sigma = 0, \quad \frac{d\xi}{d\sigma} + F_s\xi = 0; \quad \sigma = 1.$$

The mean temperature profile $\bar{T}$ enters in the function F in (1) that incorporates effects of the column static stability (F_s is the surface expression for F; for details see Silva-Dias 1986).

Solutions to the governing equation in the vertical are given as linear combinations of the eigenfunctions $\xi_n(\sigma)$ and eigenvalues D_n for the $n = 1, 2, 3, \cdots, N$ vertical modes. The phase speed c_n for each mode is a function of the eigenvalue $c_n = \sqrt{D_n}$. Individual profiles of u', v', and z' can be projected onto the vertical modes by

$$\begin{bmatrix} u_n \\ v_n \\ z_n \end{bmatrix}(\lambda, \phi, t) = \sum_{k=1}^{N} \xi_n(k) \times \begin{bmatrix} u'(\lambda, \phi, k, t)/\sqrt{D_n} \\ v'(\lambda, \phi, k, t)/\sqrt{D_n} \\ z'(\lambda, \phi, k, t)/(D_n/g) \end{bmatrix},$$

where the u_n, v_n, and z_n are the projections and the primed quantities are the profiles (over k levels) of the observations. From these projections one can form kinetic energy $K_n = (D_n/2)(u_n^2 + v_n^2)$ and available potential energy $A_n = (D_n/2)(z_n^2)$ estimates for each mode. The relative importance of each mode can then be quantified in terms of the percentage of the total energy it contains:

$$R_n = \frac{K_n + A_n}{\sum_{n=1}^{N} (K_n + A_n)} \times 100\%.$$

Note that by means of the linear approximation and the assumption of a rigid lid, we have excluded the realistic possibilities that 1) the vertical and horizontal modes are themselves dispersive and 2) energy can propagate vertically to escape the troposphere or partially reflect at the tropopause. We will discuss some implications of these assumptions in section 3.

Similar to the methodology of Silva-Dias and Bonatti (1985), sets of vertical modes ξ_n were obtained for Kanton Island and Balboa (always using the local $\bar{T}$) for 30-level profiles ($N = 30$) up to 8 hPa. The gravest of these modes did not differ significantly in either structure or eigenvalue from vertical modes obtained for the same stations using 10 equally spaced levels ($N = 10$) up to 100 hPa. The lower-resolution modes were used in the projections listed in Table 1. Projections were repeated after first bandpass filtering the station data with a filter peak centered at a 48-day period.[5] These projections should emphasize signals associated with the ITO. The percentage of energy explained by the dominant modes in the bandpass filtered case are listed in Table 2.

Not surprisingly, the dominant modes in all cases (station, season, filter) are the barotropic mode (BT) and the first baroclinic mode (1 BC) with a zero crossing near 500 hPa. The profiles of these modes at Kanton, using winter data to solve (1), are shown in Fig. 5. The theoretical phase speeds for these modes are in the neighborhood of 290 m s^{-1} for the

[5] The filter response is identical to that in Madden (1986, Fig. 4), except for the central frequency: 1/48 d^{-1} here and 1/47 d^{-1} there. The half-power points are at 1/71 d^{-1} and 1/35 d^{-1}.

barotropic mode and 50 m s^{-1} for the first baroclinic mode. Clearly we are anticipating that the surface-pressure anomaly signal associated with the ITO will be manifest in height-dependent atmospheric properties with a first baroclinic mode structure in the vertical.

To confirm this, the cross spectrum analysis introduced above was repeated using the coincident 7 years of unfiltered (in time) geopotential heights projected in turn onto the barotropic and first baroclinic modes at Kanton Island and Balboa. Figure 6a is a plot of the squared coherence and phase for the geopotential height projections onto the barotropic mode, and Fig. 6b is the corresponding plot for the first baroclinic mode projections (the frequency axis has been expanded to show only low frequencies relative to Figs. 1 and 3). In the barotropic mode case, the squared-coherence maximum is less than one-half the magnitude of the maximum in Figs. 1 and 3. The peak in Fig. 6a is displaced toward higher frequencies. In the low-frequency band where the squared coherence is statistically significant, the barotropic geopotential height projections at Balboa lead those at Kanton Island indicating westward propagation. Thus, it does not appear that the surface pressure signal of interest is related to the barotropic mode.

Conversely, in Fig. 6b, the cross spectrum for the projections of the geopotential heights onto the first baroclinic modes at Kanton Island and Balboa resembles the cross spectrum for the surface pressure in Fig. 1 and, to a lesser extent, that in Fig. 3. Squared-coherence amplitudes are still about one-half those in Figs. 1 and 3, but the phase versus frequency curve demonstrates eastward propagation (Kanton Island leads Balboa). An approximate linear dependence of phase on frequency is also suggested. This linear phase relation implies a 3-day delay between stations, which translates to a phase speed of about 39 m s^{-1}.

In summary, cross spectral analyses of geopotential heights projected onto the barotropic and first baroclinic modes indicate that the eastward propagating signal loads largely on the first baroclinic vertical structure and confirms a phase speed reasonably close to that predicted by linear theory.

TABLE 1. Percentage of total energy explained by the leading vertical modes (barotropic, first baroclinic, and second baroclinic) from projections of *unfiltered* station data onto solutions of the vertical structure equation.

Station (season)	% BT	% 1 BC	% 2 BC
Kanton Island (summer)	24.2	38.2	11.2
Kanton Island (winter)	24.2	38.1	11.7
Balboa (winter)	23.4	34.0	13.6

TABLE 2. Percentage of total energy explained by the leading vertical modes from projections of *bandpass filtered* station data onto solutions of the vertical structure equation. The bandpass filter peak corresponds to a 48-day period. The percentages in Tables 1 and 2 are averages from over 3700 projections for the period 1 December 1956–27 January 1967.

Station (season)	% BT	% 1 BC	% 2 BC
Kanton Island (summer)	24.9	55.2	6.5
Kanton Island (winter)	24.9	55.2	7.0
Balboa (winter)	30.5	36.2	13.9

d. Complex empirical orthogonal function (cEOF) analysis

The conventional cross spectrum analysis can be extended to a cEOF analysis that diagnoses both vertical structure and phase information from time series of heterogeneous data (e.g., wind and geopotential height profiles) at several stations (see Wallace and Dickinson 1972). This approach yields an estimate of the vertical structure of propagating signals independent of theory that requires the rigid-lid approximation or a linear constraint on the dynamics.

The basic cEOF recipe for our application is as follows.

1) Fourier transform 10 years of 96-day Northern Hemisphere winter segments[6] of zonal wind and geopotential-height observations taken at ten levels for the stations at Kanton Island and Balboa.

2) Construct all combinations of cospectra and quadrature spectra for each frequency, between stations, pressure levels, and data types.

3) Average the cospectra and quadrature spectra pairs over the frequency band bounded by 1/12 d^{-1} and 1/48 d^{-1}, yielding 140 degrees of freedom if each observation is independent. This frequency band is selected to capture the regions of high coherence and (approximate) linear change in phase with frequency indicated in Fig. 1. The co- and quadrature spectral matrices are normalized by the product of the square roots of the two spectra.

4) Form the 40×40 symmetric complex covariance matrix, pairing all combinations of band-averaged cospectra (real part) and quadrature spectra (imaginary part) among all data types, for each station and at every level. The diagonal of this matrix is the average variance of a given observation.

Finally, the eigenvalues and eigenvectors of this matrix are extracted by a standard package. The elements

[6] We emphasize Northern Hemisphere winter because the ITO is known to be stronger then (Madden 1986). An identical analysis has been performed with summer data, yielding results that are qualitatively very similar to those reported below.

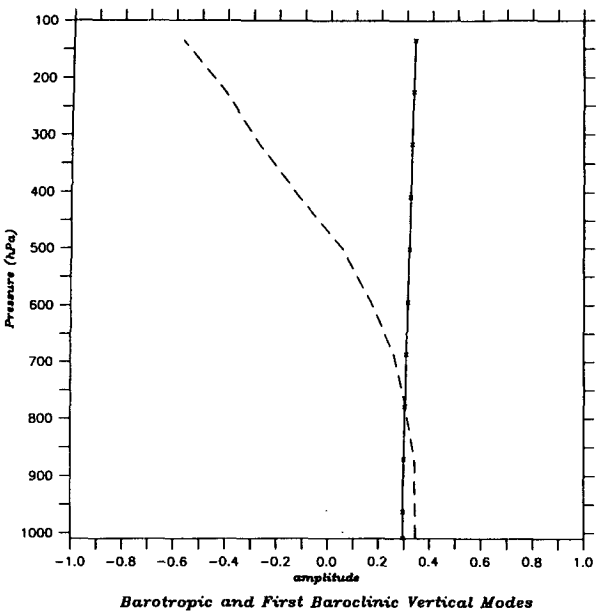

FIG. 5. Vertical profiles for the barotropic (solid line) and first baroclinic (dashed line) mode solutions to the vertical structure equation (see text). The modes were constructed from historical geopotential height and wind data from winter rawinsonde observations at Kanton Island. Barotropic and first baroclinic mode solutions for summer observations at Kanton and winter observations at Balboa are very similar in structure and amplitude to the modes depicted here. Summer modes at Balboa were not computed.

of the eigenvectors are vertical profiles of real and imaginary pairs from which we form amplitude and phase angle profiles of the vertical structure. The eigenvalues are a measure of the variance accounted for by the corresponding eigenvectors. Typically, only the first few eigenvectors account for large fractions of the variance and may be physically meaningful. In practice, the physical interpretation of the vertical structure often emerges only when the cEOF analysis is repeated for slightly different combinations of data types and/or stations (e.g., Wallace and Dickinson 1972).

The profiles associated with the dominant vertical structure are shown in Fig. 7. This leading cEOF accounts for 34% of the variance in the station data considered. To interpret this figure it makes sense to first describe the cEOF output of a wave mode that could plausibly represent the fast eastward propagation of interest. The idealized cEOF of a first baroclinic mode Kelvin wave, propagating from Kanton Island to Balboa at 40 m s^{-1}, is depicted in Fig. 8, where we have pretended that the vertical structure of the wintertime first baroclinic mode at Kanton Island (Fig. 5) captures all the variance (energy) in the data from both stations. In Fig. 8, the idealized cEOF amplitude profiles touch zero at the zero crossing level for the first baroclinic mode profile. The idealized cEOF amplitude profiles in the geopotential height and zonal winds are identical at each station. The idealized phase angle changes abruptly with pressure level at exactly the level of the vertical-mode zero crossing. In our idealized Kelvin wave case, geopotential height and zonal velocity are in phase at each station. The phases at Kanton Island are shown to lead Balboa by 0.25 cycle, corresponding to the 92° longitudinal separation and assuming zonal-wave one longitudinal structure (to be discussed below).

Comparing Figs. 7 and 8 it is clear that the variance in the real data accounted for by the dominant cEOF is different from the variance we could attribute to a simple, first baroclinic mode, equatorial Kelvin wave. However, some of the features of the profiles in Fig. 7 are comparable with Fig. 8. In Fig. 7 the amplitude profiles in geopotential height for both stations are nearly barotropic; however, the zonal velocity amplitude profiles are more suggestive of a first-mode baroclinic structure with a zero crossing near 700 hPa for Kanton Island and around 500 hPa for Balboa. The distinction between geopotential height and zonal velocity carries over to the phase angle profile. Kanton Island phase in geopotential height leads Balboa by less than 0.10 cycle at maximum, and they are collinear over part of the profile. The phase angles for zonal wind change abruptly at about 500 hPa for Balboa and at 700 hPa for Kanton Island. These jumps are near the relative minima in the zonal wind amplitude profiles and similar to that expected for a baroclinic Kelvin wave. Above the transitions in phase angles, Kanton Island zonal velocity leads Balboa by about 0.25 cycle. Below the transitions, Balboa leads by the same amount. For both Kanton Island and Balboa, the velocity phase-angle profiles lead geopotential height phases at both stations above the suggested zero-crossing levels. Below the zero-crossings, zonal velocity continues to lead geopotential height at Balboa, but the order is reversed at Kanton Island.

The leading cEOF in the real-data case differs from one idealized for a pure, first-mode, baroclinic-Kelvin wave. There is a mixture of barotropic and first baroclinic signals in the vertical structures, and the zonal velocity and geopotential heights are not in phase. Of course, the most significant cEOF could represent the variance due to a combination of physical phenomena in the frequency band of interest. To test this we repeated the recipe outlined above after first subtracting that portion of the station data that projected onto the barotropic modes for Kanton Island and Balboa as derived in the vertical-structure equation analysis. The amplitude and phase profiles for the resulting leading cEOF are depicted in Fig. 9.

The structures in Fig. 9 account for 36% of the variance remaining after the barotropic projections have been removed (35% for the summer data analysis). The profiles are more like Fig. 8 than in the full-data

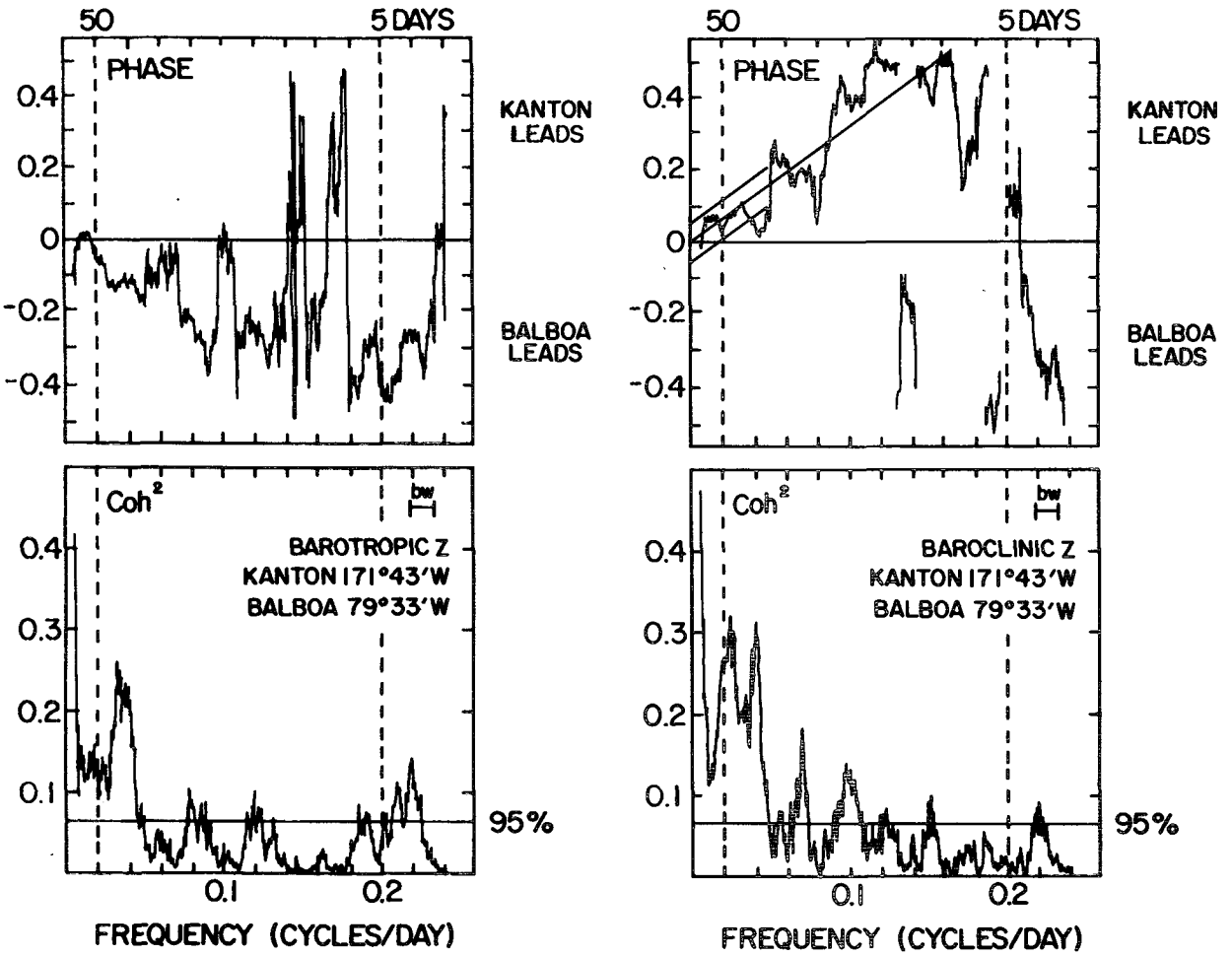

FIG. 6. (a) Coherence squared (bottom) and phase in fractions of a cycle between projections of geopotential heights onto the barotropic modes at Kanton Island and Balboa, respectively. Geopotential heights are taken from the 3700-day record over the period 1 December 1956–24 March 1967. The frequency axis has been expanded relative to Figs. 1 and 3 to emphasize low frequencies. Forty-five raw spectral estimates were averaged to yield approximately 90 degrees of freedom. The bandwidth and 95% confidence limit for coherence squared are indicated. (b) As in Fig. 6a but for projections onto the first baroclinic modes at each station. The 95% confidence interval for phase is based on an average squared coherence of 0.2 between 0 and 0.05 cpd and 90 degrees of freedom (Jenkins and Watts 1968, 381).

case (Fig. 7). The amplitude profiles for both geopotential height and zonal velocity are now similar in that they all have relative minima in the midtroposphere. At Balboa and Kanton, there are single zero crossings between 400 and 500 hPa for zonal velocity and geopotential height. Kanton Island leads Balboa in phase by about 0.10 cycle for both geopotential height and zonal velocity above and below the zero-crossing levels. Note that a rough estimate of the average phase in the statistically significant low-frequency bands in the pressure cross spectra of Figs. 1 and 3 is also about 0.10 cycle (i.e., the phase corresponding to a 30-day period).

Unlike the cEOF for the idealized Kelvin wave, the zonal velocity at each station leads the geopotential height by about 0.15 cycle (the phase difference is generally smaller in the cEOF analysis of summer data, particularly for Kanton Island). The discrepancy in phase is essentially unchanged when the cEOF analysis is repeated for a covariance matrix that also includes surface pressure data from Kanton Island and Balboa (not shown). The cEOF analysis was also repeated to include station profiles of meridional wind. If the Kelvin wave dynamical balance is the only contributor to the variance represented by the leading mode in Fig. 9, then we expect zero amplitude in the cEOF profile for the meridional velocity part. As it turns out, the amplitude for meridional velocity is about four times smaller than for zonal velocity and ten times smaller than that for geopotential height. The cEOF vertical

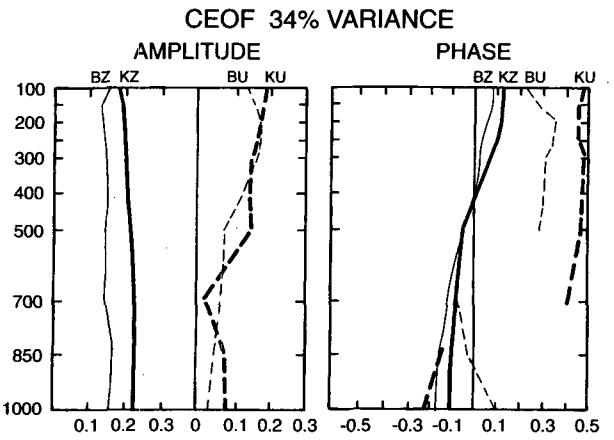

FIG. 7. Amplitude (left) and phase profiles (fractions of a cycle versus pressure) for geopotential height (Z) and zonal wind (U) at Kanton (K) and Balboa (B) as derived from the leading cEOF for the 40 × 40 covariance matrix constructed according to the recipe in the text.

structures (also not shown) for zonal velocity and geopotential height amplitudes and phases are nearly identical to those in Fig. 9. However, the total variance accounted for by the leading cEOF drops from 36% to 26% (from 35% to 27% for summer data) when meridional velocity is included in the cEOF recipe. We interpret this mixed result to indicate that while the leading mode vertical structures in Fig. 9 are robust and reminiscent of an idealized Kelvin wave signal, the contributing dynamics are more complicated than those for the Kelvin wave in isolation. Again, there is no reason to expect the cEOF procedure to separate signals as a function of dynamical mechanism.

3. Discussion

The preceding analyses of historical and recent data, using theoretical and cEOF mode decompositions, are identifying independently an eastward propagating signal, with phase speed faster than 30 m s^{-1}, in the propagating region of the equatorial Pacific. The vertical structure of this signal exhibits a single zero crossing in the midtroposphere. The signal occurs in a low-frequency band associated with the ITO. In this section we examine our simple conceptual model of a linear-dispersion relationship between the fast, eastward signal and the ITO.

It is possible that the 30–40 m s^{-1} signal we detect in the station data can be thought of as part of the response to convective forcing in general, as opposed to that specifically associated with the ITO. However, in a preliminary examination of a single event in the zonal winds from the *ERS-1* scatterometer data (not presented here), we can associate evidence of the 30–40 m s^{-1} signal with a pattern in the 200-hPa velocity potential (from weather center analyses) that is an indicator of the ITO. A more thorough exploration of the connection of the fast component to the ITO versus a connection with convection in a more general sense (see for example Salby and Hendon 1994) must await further research.

Tropospheric, first baroclinic mode vertical structure has been associated with the ITO since its discovery (Madden and Julian 1972a; e.g., see their Fig. 13). Gill (1980) demonstrated that a single tropospheric zero crossing was a natural vertical structure for the response eastward of a simple diabatic heating at the equator localized over Indonesia. Salby et al. (1994) included more realistic effects of surface friction and moisture convergence in the boundary layer at the equator to modify this simple picture. They demonstrate that surface convergence leads convergence above the surface boundary layer (say 850 hPa) by 40° to 50° in longitude. Hendon and Salby (1994) present a composite study of the ITO in the troposphere wherein a first-baroclinic mode vertical structure[7] overlies this effect in the boundary layer.

More rapid propagation in the Eastern Pacific of signals in various atmospheric properties associated with the ITO has also been noted by Hendon and Salby (1994), among many others. Hendon and Salby (1994) show that a first baroclinic structure in zonal winds from analysis fields (between 850 and 200 hPa) is linked to the convection anomalies in the Indian and Western Pacific Oceans. This signal survives and speeds up in the Eastern Pacific after the convection has died out. In Hendon and Salby (1994), the eastward propagation rate increases from about 5 m s^{-1} west of the date line where it is linked to the convection anomalies to about 10 m s^{-1} east of the date line in what we have termed the propagating region (see also Knutson and Weickmann 1987). The Hendon and Salby (1994) analysis did not include the surface pressure data that might preclude the discovery of the faster mode identified in our study. Recently, Weickmann (personal communication, 1995) has identified a fast (30–60 m s^{-1}), eastward signal in the sea level pressure from National Meteorological Center analyses of the eastern equatorial Pacific Ocean region.

The notion of forced versus propagating regions is also evident in many previous studies, including Salby and Hendon (1994). They identify a forced regime in the Indian Ocean and Western Pacific and a radiating regime in the Eastern Pacific. The concept of identifying the radiating solution with a dispersion product from the forced response is similarly not new to our

[7] Hendon and Salby (1994) do not refer to a vertical-mode structure per se, but rather refer to a structure that is out of phase between the lower and upper troposphere.

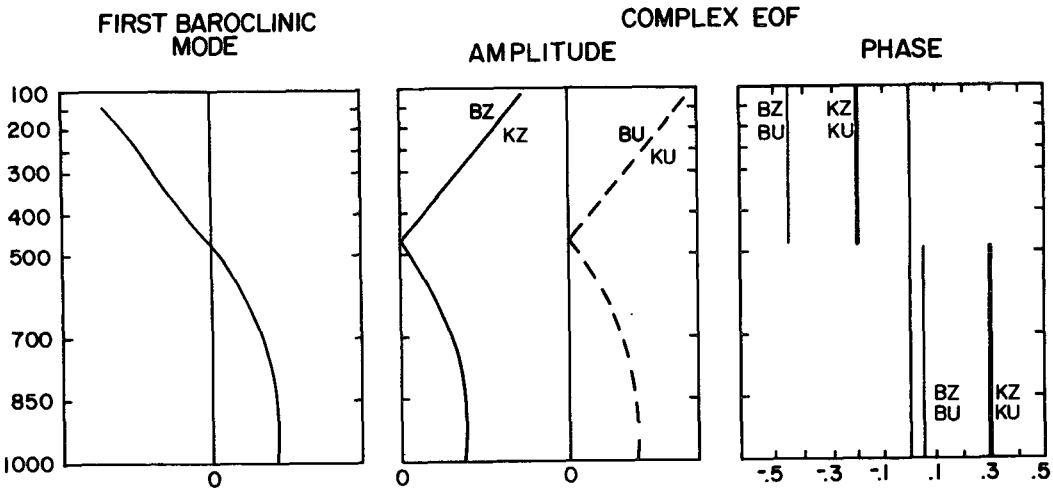

FIG. 8. Idealized amplitude (center) and phase (right) profiles from a cEOF hypothesized for a first-baroclinic mode Kelvin wave of vertical structure given by the Kanton wintertime profile (left, reproduced from the dashed curve in Fig. 5). In the idealized case, the amplitude profiles are identical in geopotential height (Z) and zonal velocity (U) at Kanton Island (K) and Balboa (B). Assuming a zonal-wavenumber one scale and a phase speed of 40 m s^{-1}, Kanton height and zonal velocity (KZ and KU) lead Balboa height and zonal velocity (BZ and BU) by 0.25 cycle as shown. The amplitude profiles go to zero and the phase profiles shift by 0.5 cycle (negative phases aloft) at the zero crossing pressure in the theoretical mode profile.

study. Chang (1977) develops a simple linear, equatorial β-plane model for Kelvin waves modified by linear damping. His solutions for eastward propagating signals are of two kinds, corresponding to the intersection of a single vertical wavenumber value with points on a dispersion curve for a given damping timescale (see his Fig. 2). At the rapid phase speed end of the curve the signals are dominated by an inertial timescale, whereas signals at the slower phase speed end of the curve are dominated by the damping timescale. For a 5-day damping time in this simple model, the fast waves exhibit a 40 m s^{-1} phase speed that is purported to be observable only in the stratosphere. Masking this signal in the troposphere is a viscous timescale signal with phase speed around 7 m s^{-1}, which is attenuated in the vertical. The author claims the fast wave is representative of the Wallace and Kousky wave (Wallace and Kousky 1968), and the slow wave corresponds to the ITO. While the Chang (1977) model is not meant to include realistic friction, nonlinearities, and/or moisture effects (see for example Salby and Garcia 1987; Salby et al. 1994), it does, however, demonstrate the theoretical feasibility of a 40 m s^{-1} eastward phase-speed for a long equatorial Kelvin wave in the atmosphere that is consistent with classical linear dispersion theory.

For a phase speed $c = 40$ m s^{-1}, the equatorial Rossby radius $\sqrt{2c/\beta}$ is about 17° latitude. This is the distance at which signals associated with the equatorial Kelvin wave have decayed to e^{-1} of the equatorial amplitude. Our analyses are detecting the signal of interest in station data from Kanton (2.8°S), Balboa (9.0°N), and Howard AFB (8.9°N), all of which are within this e-folding distance from the equator. However, the analytical form of a zonal-wave 1 Kelvin wave is not a perfect fit with the signal discovered here. The wavelengths implied by statistically significant lower frequencies (e.g., 1/48 d^{-1}), and faster estimates of the phase speed (e.g., 40 m s^{-1}) are more than four times the circumference of the earth. This suggests a waveform more complicated than a single sinusoid [as does

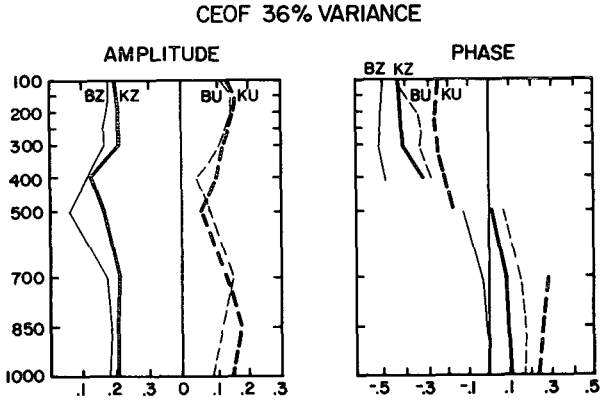

FIG. 9. Amplitude and phase profiles as in Fig. 7 from the leading cEOF for a 40 × 40 covariance matrix constructed as before from geopotential height and zonal wind observations minus their projections onto the barotropic modes for each station derived from the vertical structure equation.

the schematic in Madden and Julian (1972a)]. Our conceptual model does not account for the possibility of propagation in the vertical (or reflection from the tropopause), which could increase the apparent wavelength at the surface. But these effects are not large enough to balance a wavelength discrepancy of a factor of four.

4. Conclusions

The hint of a rapid, eastward, phase propagation in the Tropics of the Eastern Pacific was detected in the surface pressure part of a schematic describing the ITO (Madden and Julian 1972a; their Fig. 16, see also their Figs. 4 and 12). Cross spectra from both historical and modern meteorological station data at Kanton Island and Balboa (or Howard AFB) confirm the existence of an eastward propagating signal with a phase speed of about 30–40 m s^{-1}, which we associate with the surface pressure anomaly in the schematic.

Theoretical vertical modes for Kanton Island and Balboa were derived from wind and geopotential-height profiles. The leading theoretical modes in terms of percentage of energy explained were of barotropic and first baroclinic form in the troposphere. Projections of the station data (zonal winds and geopotential heights) were obtained for each of these modes at each station. Cross spectra of the projections for each mode demonstrate that the rapid eastward propagation is associated with the first baroclinic mode vertical structure and not with the barotropic mode. The phase-speed estimate from cross spectra of the first baroclinic mode projections is again about 40 m s^{-1}.

An independent verification of first baroclinic mode vertical structure and rapid eastward-phase propagation can be obtained from a cEOF analysis. A covariance matrix was constructed from station data (geopotential heights and zonal winds at Kanton Island and Balboa) minus the projections of those data onto barotropic-mode profiles from the linear theory. The leading cEOF of this matrix compares favorably with the hypothetical cEOF we idealized for a pure Kelvin wave signal propagating at 40 m s^{-1} between the two stations. The cEOF from the station data minus barotropic projection implies a single zero crossing in the midtroposphere and phase angle differences of about 0.1 cycle, with Kanton Island leading Balboa. The 0.1 cycle phase is about the average of phases between Kanton Island and Balboa in the entire range of frequencies 1/48 d^{-1} to 1/12 d^{-1} evident in the pressure cross spectrum (Fig. 1). However, in contrast to the idealized Kelvin wave, geopotential height and zonal wind are out of phase by about 0.15 cycle at both stations in this cEOF, with wind leading height.

We have invoked a conceptual model of the rapid phase-speed signal as a Kelvin wave dispersion product of the response to strong convection events in the forcing region of the equatorial troposphere. This conceptual model has been shown to be imperfect; it implies unrealistically long wavelengths in a low-frequency region of high coherence. However, a simple Kelvin wave model due to Chang (1977) does predict the existence of a fast eastward mode with a phase speed of about 40 m s^{-1}, which is purported to be masked in the troposphere by a slower, eastward mode associated with the ITO. Chang (1977) associates the faster mode in the lower stratosphere with the Wallace and Kousky (1968) wave. Our analyses of meteorological station observations indicate that the 40 m s^{-1} wave is detectable in the equatorial troposphere of the propagating region as well. This suggests a link between the ITO and the Wallace and Kousky (1968) wave that warrants further pursuit.

Acknowledgments. We thank Prof. Murry Salby for several interesting and beneficial discussions. Drs. Grant Branstator, David Gutzler, James McWilliams, Joseph Tribbia, and J. M. Wallace and Mr. Tim Hoar all provided useful input at various stages of this research. We thank Prof. Dennis Moore, Dr. Klaus Weickmann, and two anonymous reviewers for helpful comments. Recent data were obtained from Mr. Dennis Joseph of the Data Support Section at NCAR. Ms. S. Whitman drafted the figures. Ms. B. Ballard and Ms. L. Harper helped with the typing. RFM is supported through a NASA Interagency Agreement supporting the NSCAT Science Working Team at NCAR.

REFERENCES

Chang, C.-P., 1977: Viscous internal gravity waves and low-frequency oscillations in the Tropics. *J. Atmos. Sci.*, **34,** 901–910.

Gill, A. E., 1980: Some simple solutions for heat-induced tropical circulation. *Quart. J. Roy. Meteor. Soc.*, **106,** 447–462.

Gutzler, D., and R. A. Madden, 1989: Seasonal variations in the spatial structure of intraseasonal tropical wind fluctuations. *J. Atmos. Sci.*, **46,** 641–660.

Hayashi, Y., and S. Miyahara, 1987: A three-dimensional linear response model of the tropical intraseasonal oscillation. *J. Meteor. Soc. Japan,* **65,** 843–852.

Hendon, H. H., 1988: A simple model of the 40–50 day oscillation. *J. Atmos. Sci.*, **45,** 569–584.

——, and M. L. Salby, 1994: The life cycle of the Madden–Julian oscillation. *J. Atmos. Sci.*, **51,** 2225–2237.

Jenkins, G. M., and D. G. Watts, 1968: *Spectral Analysis and Its Applications.* Holden-Day, 525 pp.

Kasahara, A., and K. Puri, 1981: Spectral representation of three-dimensional global data by expansion in normal mode functions. *Mon. Wea. Rev.*, **109,** 37–51.

Knutson, T. R., and K. M. Weickmann, 1987: 30–60 day atmospheric oscillation: Composite life cycles of convection and circulation anomalies. *Mon. Wea. Rev.*, **115,** 1407–1436.

——, ——, and J. E. Kutzbach, 1986: Global-scale intraseasonal oscillations of outgoing longwave radiation and 250-mb zonal wind during Northern Hemisphere summer. *Mon. Wea. Rev.*, **114,** 605–623.

Lau, K.-M., and L. Peng, 1987: Origin of low-frequency (intraseasonal) oscillations in the tropical atmosphere. *J. Atmos. Sci.*, **44,** 950–972.

Longuet-Higgins, M. S., 1968: The eigenfunctions of Laplace's tidal equations over a sphere. *Philos. Trans. Roy. Soc. London,* Ser. A, **262,** 511–607.

Madden, R. A., 1986: Seasonal variations of the 40–50 day oscillation in the Tropics. *J. Atmos. Sci.,* **43,** 3138–3158.

——, and P. R. Julian, 1972a: Description of global-scale circulation cells in the Tropics with a 40–50 day period. *J. Atmos. Sci.,* **29,** 1109–1123.

——, and ——, 1972b: Further evidence of global-scale 5-day pressure waves. *J. Atmos. Sci.,* **29,** 1464–1469.

——, and ——, 1994: Observations of the 40–50-day tropical oscillation—a review. *Mon. Wea. Rev.,* **122,** 814–837.

Panofsky, H. A., and G. W. Brier, 1963: *Some Applications of Statistics to Meteorology.* The Pennsylvania State University Press, 223 pp.

Salby, M. L., and R. R. Garcia, 1987: Transient response to localized episodic heating in the Tropics. Part I: Excitation and short-time near-field behavior. *J. Atmos. Sci.,* **44,** 458–498.

——, and H. H. Hendon, 1994: Intraseasonal behavior of clouds winds and temperature in the Tropics. *J. Atmos. Sci.,* **51,** 2207–2224.

——, R. R. Garcia, and H. H. Hendon, 1994: Planetary-scale circulations in the presence of climatological and wave-induced heating. *J. Atmos. Sci.,* **51,** 2344–2367.

Silva-Dias, P. L., 1986: Vertical mode decomposition and model resolution. *Tellus,* **38A,** 205–214.

——, and J. P. Bonatti, 1985: A preliminary study of the observed vertical mode structure of the summer circulation over tropical South America. *Tellus,* **37A,** 185–195.

Wallace, J. M., 1972: Empirical orthogonal representation of time series in the frequency domain. Part II: Application to the study of tropical wave disturbances. *J. Appl. Meteor.,* **11,** 893–900.

——, and V. E. Kousky, 1968: Observational evidence of Kelvin waves in the tropical stratosphere. *J. Atmos. Sci.,* **25,** 900–907.

——, and R. E. Dickinson, 1972: Empirical orthogonal representation of time series in the frequency domain. Part I: Theoretical considerations. *J. Appl. Meteor.,* **11,** 887–892.